J Appl Electrochem (2009) 39:1803–1808
DOI 10.1007/s10800-009-9883-5

ORIGINAL PAPER

Pseudo-capacitance properties of porous metal oxide nanoplatelets derived from hydrotalcite-like compounds

Jun Wang · Hao Qin · Jia You · Zhanshuang Li · Piaoping Yang · Xiaoyan Jing · Milin Zhang · Zhaohua Jiang

Received: 23 August 2008 / Accepted: 26 March 2009 / Published online: 8 April 2009

Abstract Nanoplatelets of metal oxides with interesting porous structure were obtained by thermal treatment of Ni/Al hydrotalcite. Structural and surface properties of the porous oxides were characterized by X-ray diffraction (XRD), transmission electron microscopy (TEM and HRTEM), and N_2 adsorption–desorption. The electrochemical performance of the electrodes was investigated by cyclic voltammetry, electrochemical impedance spectroscopy and constant current charge–discharge measurements. Ni/Al hydrotalcite calcined at 450 °C (NA-450) displayed a maximum specific capacitance (419.0 F g^{-1}) due to the porous structure with the highest specific surface area (142.3 m^2 g^{-1}) and small pore size (4.4 nm). The present study shows the potential of NiO nanoplatelets composite material for electrochemical pseudo-capacitors.

Keywords Hydrotalcite-like compounds · Porous structure · Specific capacitance · Pseudo-capacitor

J. Wang · Z. Jiang (✉)
School of Chemical Engineering and Technology, Harbin Institute of Technology, Harbin 150001, People's Republic of China
e-mail: zhqw1888@sohu.com

H. Qin · J. You
The 49th Research Institute of China Electronics Technology Group, Harbin 150001, China

Z. Li · P. Yang · X. Jing · M. Zhang
College of Material Science and Chemical Engineering, Harbin Engineering University, Harbin 150001, People's Republic of China

1 Introduction

Oxides and hydroxides of transitional metals, such as cobalt [1, 2], iron [3] and nickel [4, 5], have attracted increasing attention owing to their potential applications in a variety of fields. Among them, nickel oxide, as one of the relatively few metal oxides with p-type semiconductivity, has been extensively investigated because of its stable band gap. Nickel oxide has received much attention over the last few years due to its large surface area and high conductivity pseudo-capacitive behavior. It can be used in catalysts [6], electrochromic films [7], fuel cell electrodes [8], electrochemical capacitors [9] and others [10, 11]. Nickel oxide is considered as one of the promising potential electrode materials for pseudo-capacitors.

Nickel oxides as pseudo-capacitor electrode materials have been synthesized using different techniques such as evaporation, coprecipitation, sol–gel techniques, sputtering and electrodeposition [12–14]. Liu et al. [15] synthesized porous nickel oxide films with the sol–gel process, but the films could only provide a specific capacitance of 50–64 F g^{-1}. Zhang et al. [16] prepared nanocrystalline NiO by a simple liquid-phase process; a specific capacitance approximately of 300 F g^{-1} was achieved. However, these synthetic processes are sophisticated and it is difficult to control the structure. Srinivasan and Weidner [17] applied an electrochemical precipitation method to fabricate NiO electrodes. In more recent work, these authors reported that the specific capacity reached 104 and 155 F g^{-1} when cycling a 350 μg NiO film over a 0.35 and 0.5 V range, respectively. But the condition is rigid and the deposition quantity was restricted by the dimensions of the electrode.

In this work, we demonstrate a simple approach to fabricate porous nickel oxide. Firstly, the single crystalline

Ni–Al hydrotalcite (NAH), as the precursor, was synthesized by a hydrothermal method. The nanoplatelets of oxide were then prepared by thermal decomposition of the Ni/Al hydrotalcite precursor. The structure and surface properties of the obtained materials were characterized by XRD, TEM and N_2 adsorption–desorption. The electrochemical performance was investigated by cyclic voltammetry, impedance and constant current charge/discharge measurements. The high specific surface area of NA-450 has significant implications with respect to energy storage devices (batteries, supercapacitors) based on electrochemical active sites and energy conversion devices (fuel cells and thermoelectric devices) depending on the catalytic site of the defect structure [18–21].

2 Experimental

2.1 Preparation of porous metal oxide electrode

The Ni/Al hydrotalcite was synthesized by a coprecipitation method at low supersaturation conditions followed by hydrothermal treatment [22]. All the chemicals were of analytical grade and were used as received without further purification. Typically, a total of 17.45 g of $Ni(NO_3)_2 \cdot 6H_2O$ and 7.5 g of $Al(NO_3)_3 \cdot 9H_2O$ were dissolved in 50 mL deionized water to form a solution, into which an aqueous solution of NaOH and Na_2CO_3 were added dropwise at 65 °C with vigorous stirring to adjust the pH to 11. Then the mixture was transferred to an autoclave pressure vessel and hydrothermally treated at 200 °C for 10 h. The autoclave was then cooled down to room temperature. The resulting solid products were separated by filtration, washed with distilled water and dried at 80 °C for 24 h. Then the Ni/Al hydrotalcite was calcined at 200, 300, 450, 550, 700, and 900 °C for 5 h, respectively. The obtained material was designated as NA-T (T is referred to as calcination temperature).

Electrodes for electrochemical capacitors were prepared by mixing 70 wt% of the oxide with 10 wt% acetylene black, 15 wt% graphite and 5 wt% polytetrafluoroethylene (PTFE). A small amount of ethanol was then added to this composite to make a more homogeneous mixture, which was pressed on nickel grid (1 cm × 1 cm). The loading of the electrode was 20 mg cm^{-2}. All electrochemical measurements were done in a three-electrode arrangement. The prepared electrode was used as the working electrode and a platinum foil of the same area as counter electrode. All potential were referred to the Hg/Hg_2Cl_2 reference electrode in the same electrolyte. All measurements were carried out in 0.5 M NaOH electrolyte.

2.2 Structural characterization and electrochemical measurement

Powder X-ray diffraction (XRD) patterns were recorded on a Rigaku D/max-IIIB diffractometer using Cu Kα radiation ($\lambda = 0.15406$ nm). The Brunauer-Emmett-Teller (BET) equation was used to calculate the specific surface area. Pore size distributions were obtained using the Barrett-Joyner-Halenda (BJH) method from the adsorption branch of the isotherm. Transmission electron microscopy (TEM) was performed on a FEI Tecnai G2 S-Twin electron microscope with an acceleration voltage of 200 kV. Samples were dispersed in ethanol. Carbon-coated copper grids were used as the sample holder. Electrochemical performance was evaluated by cyclic voltammetry (CV) using a IM6eX electrochemical workstation made in Germany. The voltage scan rate was 5 mV s^{-1}. The galvanostatic charge/discharge of the electrodes was evaluated using a Chenhua CHI760C electrochemical workstation (Shanghai, China) at room temperature.

3 Results and discussion

3.1 Material characterization

The XRD patterns of Ni/Al hydrotalcite calcined at different temperatures are displayed in Fig. 1. The characteristic reflections of the typical hydrotalcite-like compounds are clearly observed for the sample calcined at 200 °C, which indicates the existence of the lamellar structure of hydrotalcite. The (003) and (006) reflections locate at 2θ of 11.4° and 22.8° respectively. When the temperature increases to 300 °C, the (003) reflection shifts to higher angle. This may

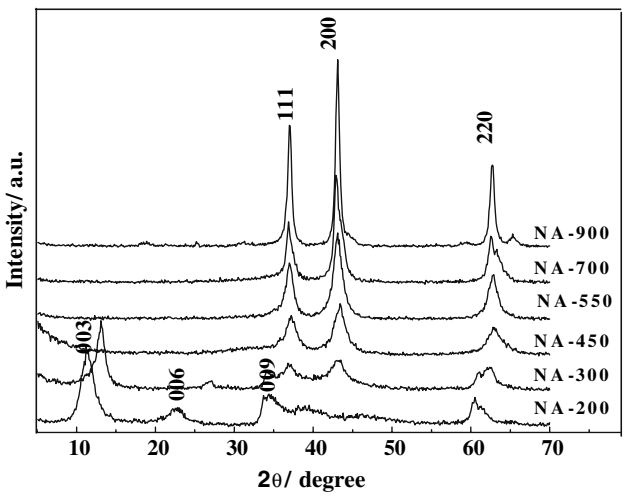

Fig. 1 XRD patterns of NAH precursor calcined at different temperatures

be due to the decomposition of the hydroxide layers. It should be noted that the characteristic (111) and (200) reflections of NiO appear at this temperature and the increase in calcination temperature leads to the decomposition of NAH precursor and the formation of single NiO (cubic structure, JCPDS 4-835). When the temperature increases to 450 °C, the (111), (200) and (220) diffraction peaks of NiO can be clearly seen. With further increase in calcination temperature, the diffraction peaks become narrower and more intense; this can be attributed to the growth of crystallites and improvement of crystallization. The Al^{3+} ions can either be incorporated in an amorphous nickel aluminate phase, or in a separate amorphous alumina phase [23]. For the conventional Ni–Al HTLcs, a nickel aluminate spinel ($NiAl_2O_4$) is formed as a crystalline phase at 800 °C. However, for our sample, even though temperature is increased to 900 °C, the sample still possesses the single NiO crystalline phase. This can be ascribed to the hydrothermal treatment. The single NiO crystalline phase maintained at this temperature is particularly important for applications in catalysis and electrochemistry.

The SEM and TEM images of NAH precursor are shown in Fig. 2a and b, respectively. The sample consists of relatively uniform hexagonal platelet-like sheets. Figure 2c–e shows the TEM images of NA-450 at different magnifications and the corresponding Fourier-filtered transformed (FFT) (inset) image. On the basis of the XRD and TG-DSC results, the hydroxide precursor calcined at 450 °C results in the complete decomposition of NAH precursor and the formation of nanoporous metal oxide as shown in Fig. 2c. A higher magnification of the porous nanoplatelets is shown in Fig. 2d. The image clearly shows the large pores formed by the aggregation of the nanoparticles. The pore diameter is about 3–4 nm, which can be attributed to the loss of hydroxyl ions and removal of carbonate ions from the hydrotalcite interlayer. The surface properties can be further demonstrated by N_2 adsorption–desorption analysis. Moreover, the lattice fringes can be easily observed from the HRTEM image. The lattice fringe corresponding to (200) ($d = 0.21$ nm) and (111) ($d = 0.24$ nm) crystallographic planes of NiO are presented in Fig. 2e. The result is consistent with the Fourier diffractogram shown in the inset of Fig. 2e.

In order to study the influence of calcination temperature on the textural properties of Ni/Al hydrotalcite, N_2 adsorption/desorption test was studied and the results are given in Table 1. As seen in Table 1, the surface area of the samples changes gradually with increase in calcination temperature. This result may be attributed to the different aggregation formats of primary particles (constituent crystallites) during the crystallization process. It is worth noting that the NA-450 sample possesses the largest BET surface area (142.3 $m^2\ g^{-1}$). The high specific surface area has significant implications with respect to energy storage devices (batteries, supercapacitors) based on electrochemical active sites and energy conversion devices (fuel cells and thermoelectric devices) depending on the catalytic sites of defect structure.

The BJH pore size distribution curves demonstrate that the obtained materials possess narrow pore size distribution. The average pore diameter of the NA-450 from the BJH desorption branch is about 4.4 nm, consistent with the TEM observation. The values of pore volume are observed to increase from 0.05 to 0.42 $cm^3\ g^{-1}$ with the temperature increasing from 200 to 550 °C. It can be conclude that the removal of layered water and carbonate lead to the increase in pore volume below 550 °C. At higher calcination temperature (700 °C) the values of pore volume decrease; this can be ascribed to the formation of oxide accompanied by sintering and aggregation.

3.2 Electrochemical properties

The cyclic voltammetry (CV) responses of different electrode materials at a scan rate of 5 mV s^{-1} are shown in Fig. 3. Voltammetry was carried out at potentials between 0 and 0.58 V using 0.5 M NaOH aqueous electrolyte. All samples present the clear faradaic pseudo-capacitance behavior, expected for a pseudo-capacitor. The clear redox peaks may be attributed to the oxidation and reduction of metal ions on the oxide surface. The NA-450 sample shows a maximum capacitance value, which can be ascribed to its large BET surface area and small grain size. Furthermore, the unique nanostructure of calcined hydrotalcites favours ionic transfer as well as provides high specific surface area for charge storage. The reduction peak potential (*Vc*), the oxidization peak potential (*Va*) and the oxygen evolution potential (*Vo*) are given in Table 2. The difference between *Vc* and *Va* for NA-450 is 0.077 V, which is less than for the others. The result indicates that NA-450 sample has good electrochemical reversibility. Hence, further electrochemical tests are focused on the NA-450 electrode material.

Figure 4 shows CV curves of the NA-450 electrode in 0.5 M NaOH solution at potential scan rates of 5, 10, 20 and 30 mV s^{-1} in the range 0–0.58 V. As the scan rate increases, the potential difference between anodic and cathodic peak, as well as the current density, increase. The shape of the CV curves reveals that the capacitive characteristic is distinguished from that of the electrical double layer capacitance, normally closing to an ideal rectangular shape. Because solution and electrode resistance can distort the current response at the switching potential and this distortion is dependent upon the scan rate [24], the shape of the CV curves changes when the scan rate increases. Such a result indicates that the measured capacitance is mainly based on the redox mechanism.

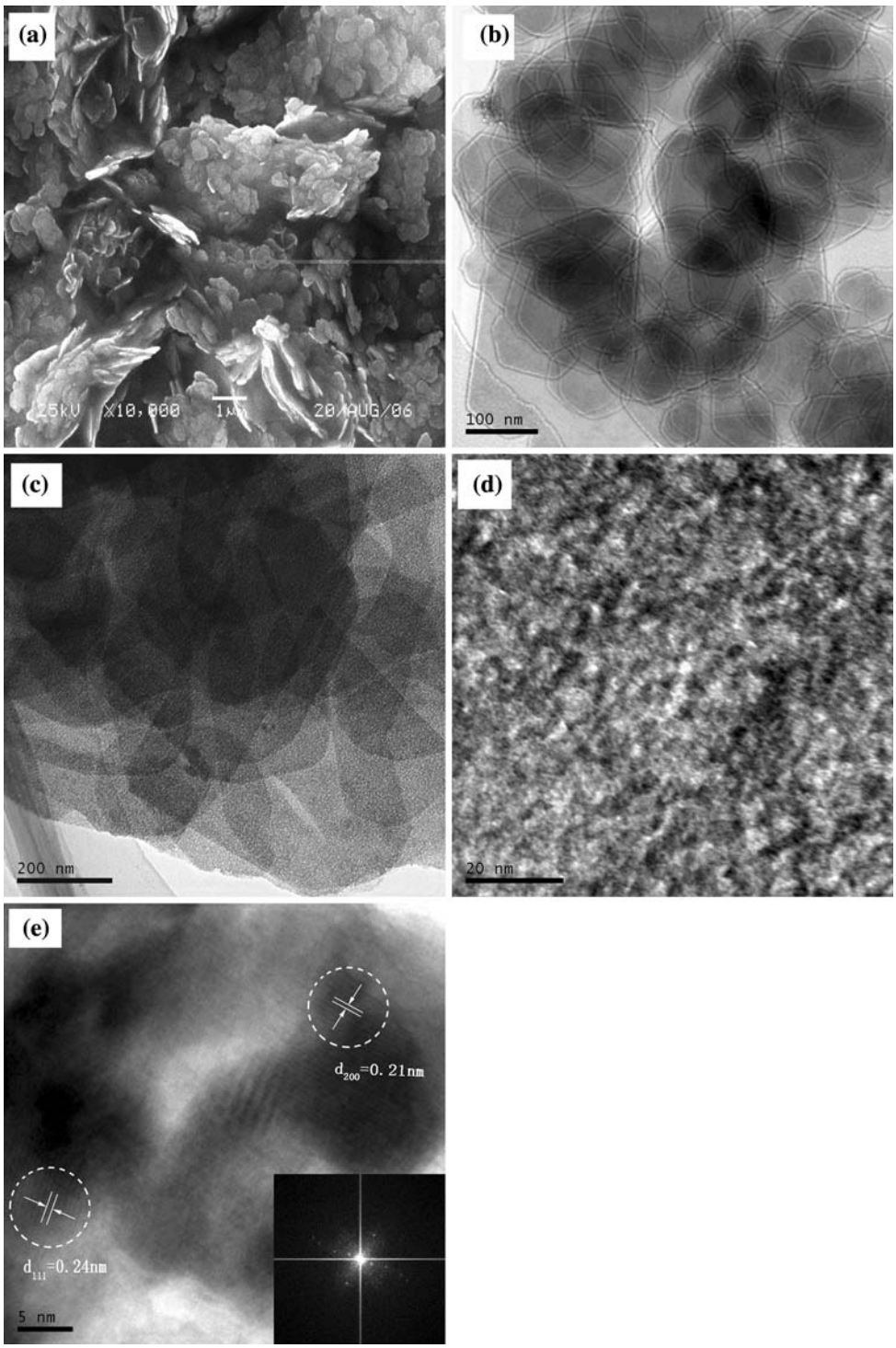

Fig. 2 The SEM and TEM images of NAH precursor (**a**, **b**) and TEM images of NA-450 at different magnifications (**c**, **d** and **e**)

Figure 5 shows the charge/discharge capacity curve of a NA-450 electrode in 0.5 M NaOH solution at a large current density of 50 mA cm^{-2}. The shape of the discharge curve does not show the characteristic of a pure double layer capacitor or pure supercapacitor, in agreement with the result of the CV curve. The specific capacitances of oxides formed at different calcination temperatures are calculated from Eq. 1, where I is the constant discharging current, Δt is the discharging time, ΔV is the potential drop during discharge, and m is the mass of the oxide. It should be noted that the specific capacitance of NA-450 obtained from the discharge curves is 419.0 F g^{-1} which is much higher than that for the NiO-based composite electrode with RuO_2 [15]. The high electrochemical performance of

Table 1 Textural properties and N_2 adsorption/desorption data of the composite oxide

Calcination temperature (°C)	Surface area ($m^2\ g^{-1}$)	Pore volume ($cm^3\ g^{-1}$)	Pore diameter (nm)
200	13.77	0.05	6.8
300	105.16	0.38	4.8
450	142.30	0.40	4.4
550	119.59	0.42	8.7
700	60.31	0.09	1.7

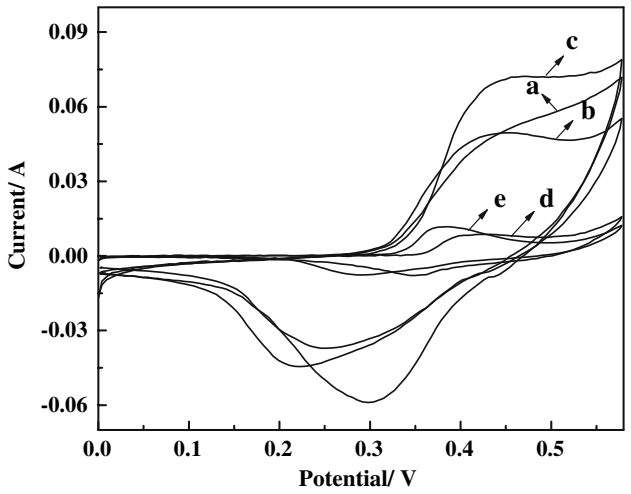

Fig. 3 CV curves of NA-200, NA-300, NA-450, NA-550 and NA-700 samples electrodes, at a scan rate of 5 mV s^{-1} in 0.5 M NaOH solution

Table 2 Characteristic potentials (V) of oxide formed at different calcination temperatures

Calcination temperature (°C)	*Vc*	*Va*	*Vo*	*Va* − *Vc*	*Vo* − *Va*
200	0.220	0.460	0.580	0.240	0.120
300	0.249	0.452	0.580	0.203	0.128
450	0.349	0.426	0.580	0.077	0.154
550	0.292	0.383	0.580	0.091	0.197
700	0.299	0.447	0.580	0.148	0.133

Vc is the potential of reductive peak

Va is the potential of oxidizing peak

Vo is the potential of oxygen inhalation

the NA-450 electrode can be ascribed to the larger BET surface area and the unique porous nanostructure.

$$Cs = \frac{I\Delta t}{m\Delta V} \quad (1)$$

Figure 6 shows the discharge curves of the NA-450 electrode at different current densities of 50, 70, 80, 90 and 100 mA cm^{-2} in a three-electrode system. The cut-off voltage of discharge is 0–0.58 V. All the curves obviously display two variation ranges. The linear variation of the

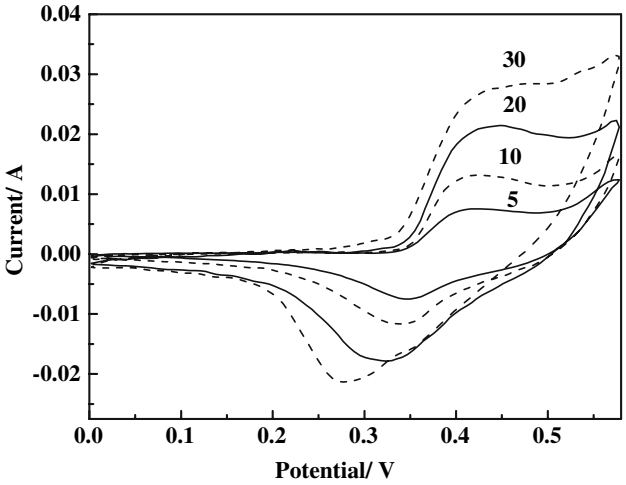

Fig. 4 CV curves of NA-450 sample in 0.5 M NaOH. Scan rates (mV s^{-1}) are indicated

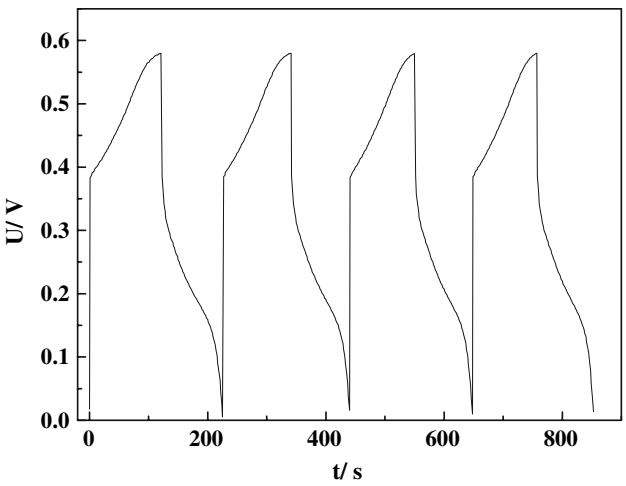

Fig. 5 Charge/discharge curve of NA-450 electrode in a voltage range from 0 to 0.58 V at room temperature. The charge/discharge current was set at 0.05 A

time dependence of the potential (below about 0.15 V) indicates the double-layer capacitance behavior, which is caused by charge separation taking place between the electrode and electrolyte interface. The slope variation of the time dependence of the potential (from 0.58 to 0.15 V) indicates a typical pseudo-capacitance behavior, which results from the electrochemical adsorption/desorption or redox reaction at the interface between electrode and electrolyte [25]. The specific capacitance of the NA-450 electrode decreases from 419.0 to 287.6, 272.3, 237.9 and 218.2 F g^{-1} as the current density increases from 50 to 70, 80, 90, and 100 mA cm^{-2}, respectively. The highest specific capacitance (419.0 F g^{-1}) was obtained at a current density of 50 mA cm^{-2}.

Electrochemical impedance spectroscopy (EIS) measurements were carried out at a dc bias of 0 V over the

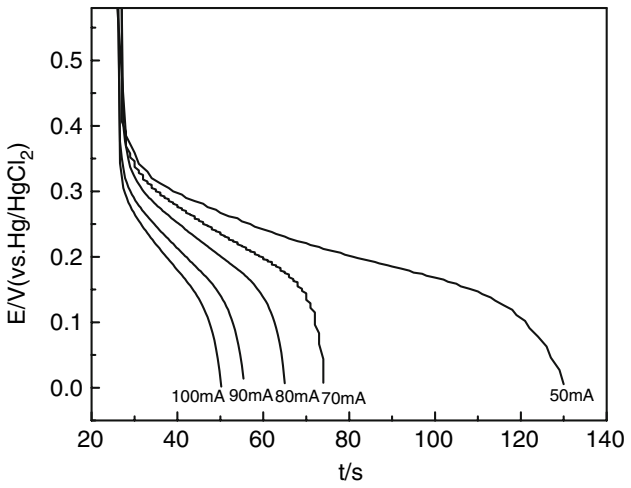

Fig. 6 Discharge curves in the potential range from 0 to 0.58 V at different discharging currents

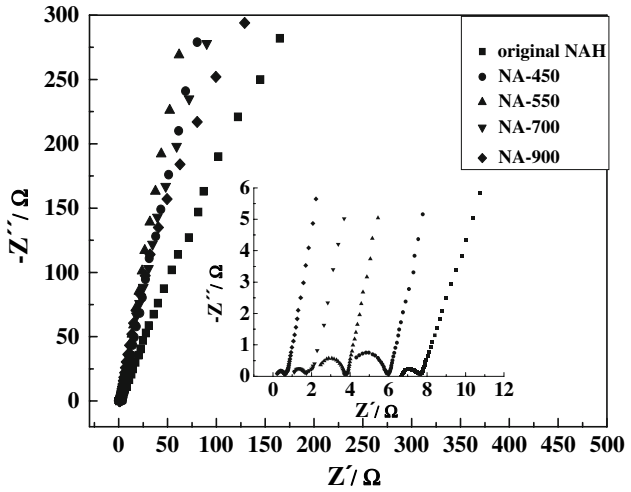

Fig. 7 Impedance plots of Ni–Al hydrotalcite calcined at 450, 550, 700 and 900 °C, respectively

frequency range 50 mHz to 100 kHz. Figure 7 presents impedance plots for the Ni–Al hydrotalcite calcined at different temperatures. At lower frequency, the imaginary part of impedance sharply increases. This represents the capacitive behavior of electrode. The straight line represents diffusion of protons within the electroactive material and pure capacitance at low frequency. The impedance plot should theoretically be a vertical line, parallel to the imaginary axis. In fact, a difference between this theoretical behavior and experimental is observed. The impedance behaviors of all the oxides come close to that of an ideal capacitor. A slight variation from the ideal capacitive behavior may be attributed to the pore size distribution of the porous oxide nanostructure. The presence of a small semicircular loop for electrodes at higher frequencies is due to the charge-transfer resistance of the electrode [26].

4 Conclusions

Nickel oxides with porous structure prepared by thermal treatment on Ni/Al hydrotalcite show a high pseudo-capacitive behavior. TEM and N_2 adsorption–desorption results show that the NAH-450 sample with nanoporous structure possesses highest specific surface area and small pore size, which result in a high capacitive property. The NA-450 sample displays a maximum specific capacitance of 419.0 F g^{-1} in 0.5 M NaOH solution. This makes it suitable for use as electrode material in electrochemical capacitors.

Acknowledgements We gratefully acknowledge the support of this research by the Key Technology R&D program of Heilongjiang Province (No. G202A423, No. TB06A05) and Science Fund for Young Scholar of Harbin City (No. 2008RFQXG028).

References

1. Xu ZP, Zeng HC (1999) Chem Mater 11:67
2. Kurmoo M (1999) Chem Mater 11:3370
3. Patrice R, Dupont L, Aldon L et al (2004) Chem Mater 16:2772
4. Nelson PA, Elliott JM, Attard GS et al (2002) Chem Mater 14:524
5. Palombari RJ (2003) Electronal Chem 546:23
6. Berchmans S, Gomathi H, Rao GP (1995) J Electroanal Chem 394:267
7. Chigane M, Ishikawa M (1992) J Chem Soc Faraday Trans 88:2203
8. Tomczyk P, Mordarski G, Oblakowski J (1993) J Electroanal Chem 353:177
9. Huang QH, Wang XY, Li J et al (2007) J Power Sources 164:425
10. Kitao M, Izawa K, Urabe K et al (1994) J Appl Phys 33:6656
11. Yoshimura K, Miki T, Jpn Tanemura S (1995) J Appl Phys 34:2440
12. Natarajan C, Matsumoto H, Nogami G (1997) J Electrochem Soc 144:121
13. Surca A, Orel B, Pihlar B et al (1996) J Electroanal Chem 408:83
14. Liu XM, Zhang XG (2004) Electrochimica Acta 49:229
15. Liu KC, Anderson MA (1996) J Electrochem Soc 143:124
16. Zhang F, Zhou Y, Li H (2004) Mater Chem Phys 83:260
17. Srinivasan V, Weidner JW (2000) J Electrochem Soc 147:880
18. Li N, Patrissi CJ, Che G et al (2000) J Electrochem Soc 147:2044
19. Spahr ME, Bitterli PS, Nesper R et al (1999) J Electrochem Soc 146:2780
20. Li N, Martin CR, Scrosati B (2000) Electrochem Solid State Lett 3:316
21. Shen CM, Zhang XG, Zhou YK et al (2003) Mater Chem Phys 78:437
22. Sharma SK, Kushwaha PK, Srivastava VK et al (2007) Ind Eng Chem Res 46:4856
23. Pérez-Ramírez J, Mul G, Moulijn JA (2001) Vib Spectrosc 27:75
24. Jiang JH, Kucernak A (2002) Electrochim Acta 47:2381
25. Zhao DD, Bao SJ, Zhou WJ et al (2007) Electrochem Commun 9:869
26. Scavetta E, Berrettoni M, Nobili F et al (2005) Electrochimica Acta 50:3305